RAPID COMMUNICATIONS

PHYSICAL REVIEW C VOLUME 46, NUMBER 6 DECEMBER 1992

Mass asymmetry, equation of state, and nuclear multifragmentation

Hong Ming Xu

Cyclotron Institute, Texas A&M University, College Station, Texas 77843

(Received 11 September 1992)

Multifragmentation is observed with an improved Boltzmann-Uehling-Uhlenbeck model for ^{40}Ar+^{51}V and ^{92}Mo+ ^{92}Mo collisions. For ^{12}C induced reactions, however, a single residue is observed up to energy $E/A \approx 200$ MeV. By investigating the dependence on the masses of the projectile and target and on the equation of state, we demonstrate that the dynamics of compression and expansion, rather than the thermal excitation energy, plays the dominant role in causing the observed multifragmentation.

PACS number(s): 25.70.Pq, 21.65.+f

Experimental investigations on the decay of hot nuclei have reported striking observations. For Ar induced reactions, cross sections for evaporation and fission residues appear to vanish at energies in excess of $E/A \approx 35$–40 MeV [1, 2]. In contrast, for carbon induced reactions, fission has been observed up to energies as high as $E/A = 84$ MeV [3]. More recently, multifragment emission is observed for Ar, Ca, and Xe [4–7] induced reactions and the average number of intermediate-mass fragments is larger for Xe than that for Ar or Ca induced reactions.

At present, the underlying mechanism for multifragment emission is still not clear and scenarios based on statistical decay, both sequential [8,9] and simultaneous [10, 11], as well as dynamical instabilities [12–25], have been modeled. For example, based on systematics of incomplete fusion, Auger *et al.* argued that the observed mass dependence of decay channels could be interpreted as a manifestation of the maximum excitation energy that hot nuclei could sustain [2]. In contrast, based on time-dependent Thomas Fermi and percolation models [14], as well as molecular dynamics and restructured aggregation models [22], Nemeth *et al.* showed that the compression energy was more efficient than the thermal energy in causing the nuclei to disintegrate. Similar results were also obtained from the time-dependent Hartree-Fock [15] and Landau-Vlasov [16–19] calculations. Recently, based on the Landau-Vlasov model, Garcias *et al.* [24] were able to explore the parameter space of energy and angular momentum, and they observed all the decay channels including evaporation, fission, and multifragmentation. In these previous calculations, however, the entrance channel leading to the formation of the hot nuclei has not been followed.

To study the mass dependence of multifragment disintegration and the dependence on equation of state (EOS), we have performed improved Boltzmann-Uehling-Uhlenbeck (BUU) calculations [26–28]. We find that the decay channel of a hot nucleus depends strongly on the mass asymmetry of the projectile and target. We show that this dependence is mainly caused by the dynamics of compression and expansion, rather than the thermal instability. The predicted decay channel is also sensitive to the EOS at the later expansion stages. Systems governed by softer EOS are more likely to break up.

We simulate the Boltzmann-Uehling-Uhlenbeck equation [29]

$$\frac{\partial f_1}{\partial t} + \mathbf{v}\cdot\nabla_r f_1 - \nabla_r U\cdot\nabla_p f_1 = \frac{4}{(2\pi)^3}\int d^3k_2\, d\Omega \frac{d\sigma_{nn}}{d\Omega} v_{12}[f_3 f_4(1-f_1)(1-f_2) - f_1 f_2(1-f_3)(1-f_4)] \quad (1)$$

with the lattice Hamiltonian method of Lenk and Pandharipande [30]. In Eq. (1), $\frac{d\sigma_{nn}}{d\Omega}$ and v_{12} are the in-medium cross section and relative velocity for the colliding nucleons, and U is the total mean-field potential consisting of the Coulomb potential and a nuclear potential with isoscalar and symmetry terms [26–28] In our calculations, we use two parameter sets [29] for the EOS which correspond to values of nuclear compressibility at K=200 MeV (soft EOS) and K=375 MeV (stiff EOS), respectively. For simplicity, $\sigma_{NN} = \int \frac{d\sigma_{nn}}{d\Omega} d\Omega$ is chosen to be isotropic and energy independent [29]. The mean-field and the Pauli-blocking factors in the collision integral are averaged over an ensemble of 80 parallel simulations.

Typical examples of our calculations are shown in Figs. 1 and 2 for ^{92}Mo+^{92}Mo, ^{12}C+^{51}V, and ^{40}Ar+^{51}V collisions. For ^{92}Mo+^{92}Mo collisions at E/A=75 MeV, $b = 0$ (Fig. 1), and calculated with the soft EOS, a compressed state is formed at $t \approx 30$ fm/c. This compressed state expands nearly isotropically and develops quickly into what appears to be a genuine multifragmentation, with fragments of similar sizes distributed on the surface of an expanding hollow sphere. To see the dependences on the equation of state, we show in Fig. 2 the top view of ^{40}Ar+^{51}V collisions (left-hand panels) at E/A=75 MeV, b =0, t = 240 fm/c, for both the soft EOS (central two panels, with different initializations) and the stiff EOS (bottom panel). For the soft EOS at this energy one always observes 3 or 4 fragments. For the stiff EOS, however, one sees a well-defined single residue in the final state. The right-hand panels of Fig. 2 show the top view of head-on collisions for an even lighter system, ^{12}C+^{51}V, calculated with the soft EOS, but at higher

energies, E/A =75 (second panel from top), 150 (third), and 200 (bottom) MeV. For this system, one always see a well-defined residue up to the highest energy calculated. The dependence on the EOS and on the masses of the colliding systems immediately suggests that it is the different dynamics of compression and decompression (or expansion), rather than the thermal excitation or rotation, that causes the multifragmentation. Since ^{12}C+^{51}V collisions at $E/A \approx 120$ MeV have approximately the same available excitation energy per nucleon as that for ^{40}Ar+^{51}V collisions at $E/A \approx$75 MeV, the fact that the systems for C induced reactions do not multifragment at much higher energies suggests that the dynamics of compression and expansion must have played a role.

To see this more clearly, we show in Fig. 3 the evolution of the average density, defined as $\langle\rho\rangle = \int_D \rho^2 d^3r/(\int_D \rho d^3r)$ [19], as a function of time. Here D indicates regions of $\rho \geq 7\%\rho_0$. The top panel shows the comparisons at a given incident energy, E/A =75 MeV. For ^{12}C+^{51}V collisions (dotted lines), the system exhibits a behavior similar to a damped monopole oscillation [18], with negligible maximum compression, $\langle\rho\rangle_{\max} \leq 1.1\langle\rho_0\rangle$, at $t \approx 25$ fm/c and modest maximum expansion, $\langle\rho\rangle_{\min} \approx 0.5\langle\rho_0\rangle$, at $t \approx 60$ fm/c. In contrast, for ^{40}Ar+^{51}V collisions calculated with the soft EOS (dashed lines), where multifragmentation is observed, the system is first compressed to $\langle\rho\rangle_{\max} \approx 1.25\langle\rho_0\rangle$ at $t \approx 25$ fm/c. It then expands substantially to very low densities, $\langle\rho\rangle_{\min} \leq 0.15\langle\rho_0\rangle$, at $t \approx 100$ fm/c. Afterwards, the density increases gradually, reflecting the condensation from a dilute system into several individual fragments. Hence the onset of multifragmentation could be viewed as a result of the gradual disappearance of damped oscillations when compression and expansion are increased. Indeed, if the system is stressed to beyond its limits to restore to a single system, it will break up into several fragments. This is clearly illustrated in the central panel of Fig. 3, where we display calculations for the same system, ^{40}Ar+^{51}V, but at different energies E/A= 35 (dotted lines), 55 (solid lines), and 75 (dashed lines) MeV, respectively. As the energy is increased, compression, and, particularly, expansion become larger. As a result, the oscillation mechanism shown at low energies disappears when the system expands to $\langle\rho\rangle_{\min} \leq 0.15\langle\rho_0\rangle$ at energies E/A=75 MeV. This result is further supported by calculations for ^{12}C+^{51}V collisions shown in the bottom

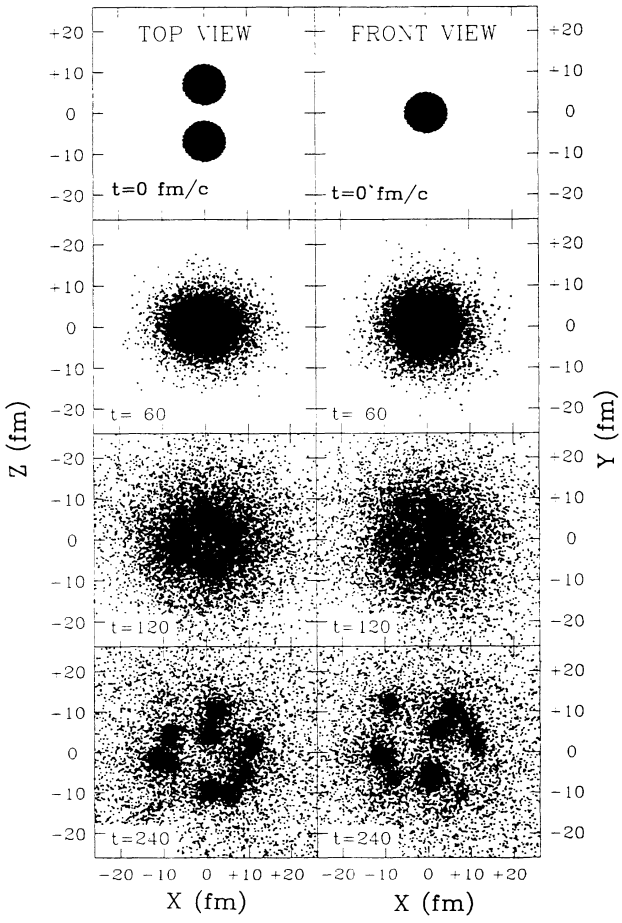

FIG. 1. BUU calculations with the soft EOS for ^{92}Mo+^{92}Mo collisions at E/A=75 MeV, b = 0. From top to bottom are time steps of 0, 60, 120, 240 fm/c, respectively. The top and front views are shown in the left and right panels, respectively.

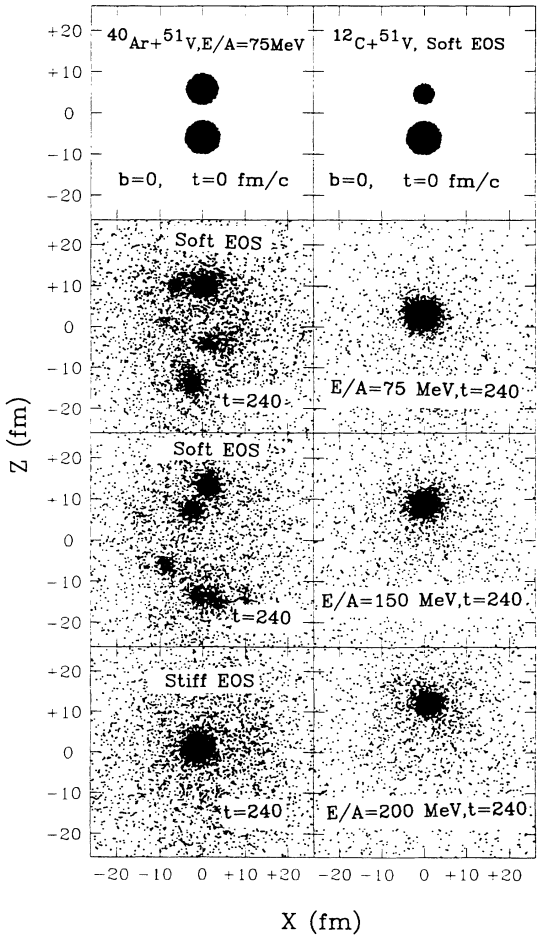

FIG. 2. The top view of BUU calculations for ^{40}Ar+^{51}V (left panels) and ^{12}C+^{51}V (right panels) collisions. Details are discussed in the text.

panel of Fig. 3, where oscillations persist up to energy $E/A \approx 200$ MeV for which no fragmentation is observed.

It is tempting to ask whether there is a critical compression or expansion for which multifragmentation channel opens up. To answer this question, we show in the top panel of Fig. 3 calculations for ^{40}Ar+ ^{51}V collisions with the stiff EOS (solid lines), where single residues are formed at E/A=75 MeV. Although the final states are completely different (see Fig. 2), similar maximum densities are reached for both the stiff and the soft EOS's. The difference, however, becomes noticeable during the later expansion stages which lead to completely different final configurations. Thus it is mainly the property of EOS at the later expansion stages that determines the final multifragmentation. Stiffer EOS has a larger surface tension and therefore its tendency for a system to break up becomes less [26]. Although it appears too early to determine a critical compression, it may nevertheless be possible to determine a critical maximum expansion since the major dynamical process is already over when the system reaches the maximum expansion. For such purpose, we have performed extensive calculations with the soft EOS for ^{40}Ar + ^{51}V collisions at different energies. We find that the critical minimum density for the system to break up appears to be very low, $\rho = 0.15\rho_0$. Further calculations indicated similar values for ^{12}C+^{51}V and ^{92}Mo+^{92}Mo systems. It is interesting to note here that this critical value is consistent with the standard value of $\frac{1}{6}\rho_0$ used to reproduce multifragmentation data [6] using the statistical fragmentation model [11].

To assess the role of thermal excitation, we have decomposed the *transverse* excitation energy approximately into three components: energy associated with compression or expansion, $E^*_{\rm exp}$ [31], collective energy, $E^*_{\rm coll}$ [32], and thermal energy, $E^*_{\rm the}$, respectively, using a technique similar to that outlined in Ref. [18], but considering only the transverse components [33]. In this decomposition, $E^*_{\rm exp}$ represents the energy change when the density distribution of the system is changed away from that of a ground state nucleus (e.g., the creation of surfaces due to fragmentation). As shown in Fig. 4, both the collective energies, $E^*_{\rm coll}/A_{\rm res}$ (central panel), and the thermal energies, $E^*_{\rm the}/A_{\rm res}$ (bottom panel), reach maximum values at $t \approx$40–50 fm/c. As a result, the systems expand and the energies stored in density, $E^*_{\rm exp}/A_{\rm res}$ (top panel), reach maximum values at slightly later times. Clearly, the maximum energies per nucleon associated with collective expansion, both $E^*_{\rm exp}/A_{\rm res}$ and $E^*_{\rm coll}/A_{\rm res}$, are much larger for the ^{40}Ar+^{51}V system than that for the ^{12}C+^{51}V sys-

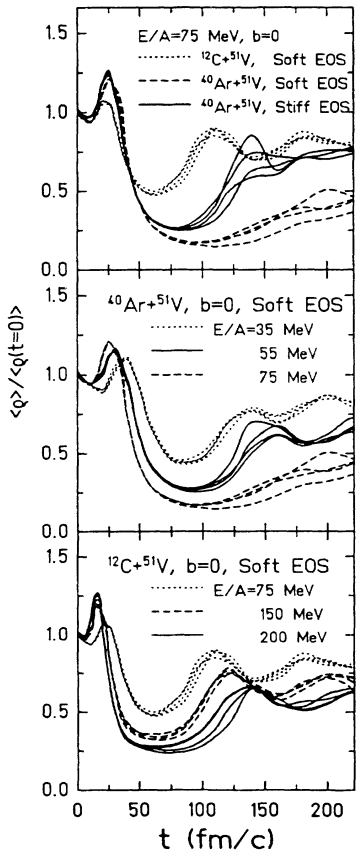

FIG. 3. The average density as a function of time. For each set of parameters, four trajectories corresponding to different initializations are displayed. For details, see the text.

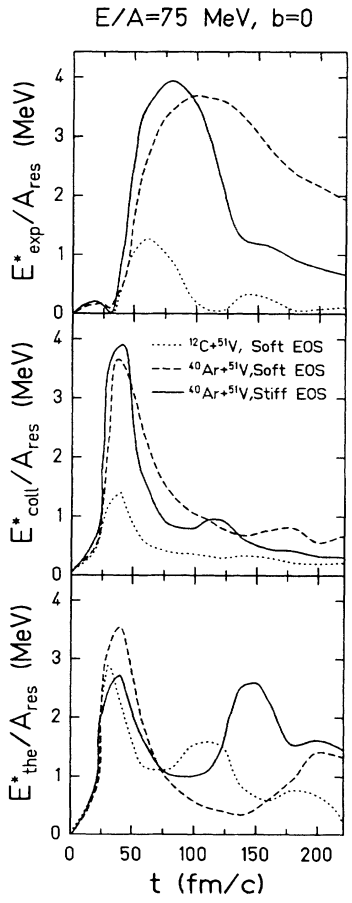

FIG. 4. The decomposition of transverse excitation energy into energies associated with expansion (top panel), collective (center), and thermal (bottom) energies for ^{40}Ar+^{51}V collisions with both the stiff (solid lines) and the soft (dashed lines) EOS's and for ^{12}C+^{51}V collisions with the soft EOS (dotted lines). For details, see the text.

tem, independent of equations of state. In contrast, similar maximum thermal excitation energies per nucleon are reached for both ^{12}C and ^{40}Ar induced reactions at $t \approx$ 40–50 fm/c. This suggests that the dynamical and collective expansion, rather than the thermal excitation, plays the dominant role for multifragmentation processes. In fact, the oscillating nature of reactions is also reflected in the thermal excitation energy (bottom panel), for which systems that suffer larger compression and expansion restore back at later times.

In conclusion, with an improved BUU model, we have studied effects of mass asymmetry in nuclear multifragmentation processes. By following the entrance channel which leads to the formation of a hot nucleus, we find that the decay pattern of a hot nucleus depends strongly on the mass asymmetry of the projectile and target. For C induced reactions, we find that the evaporation residue is the dominant reaction channel and this channel persists up to energies as high as $E/A \approx 200$ MeV. In contrast, for Ar or Mo induced reactions, multifragmentation indeed occurs at modest energies. We demonstrate that this dependence on the mass asymmetry is caused by the dynamics of collective compression and expansion, rather than the thermal instability. This result of compression and expansion, which is particularly important for heavier systems, is consistent with earlier studies [14–16,22] of the decay of hot nuclei where the entrance channel leading to their formation was not followed. It is also consistent with recent observations that statistical models that include expansion [5–8] or assume occurrence of multifragmentation at low densities [6,11] provide better agreement with experimental data, and thus provides additional support for such treatments. The predicted decay patterns are sensitive to the EOS during the later expansion stages. Systems governed by the soft EOS tend to break up more easily than those governed by the stiff EOS. Based on our calculations, we propose that, in addition to multifragmentation studies, measurements of evaporation residues in light nuclei (e.g., ^{12}C,^{14}N, etc.) induced reactions at high incident energies would provide an additional tool to pin down the roles of compression and thermal energies.

Obviously our results are based on a BUU model (mean-field + two-body collisions) and could suffer from its effective truncation by ignoring higher-order many-body dynamics, particularly when real fragmentation sets in due to large many-body correlations and fluctuations. Because of the lack of such correlations and fluctuations, the fragments formed in the BUU calculations after the onset of multifragmentation ($t_{\rm onset} \approx 120$ fm/c) may not be viewed literally as realistic fragments. However, like other effective equations of motion for reduced observables, if conditions are met, the model can signal the instabilities, even if small perturbations [34] are provided. Because BUU has been proved to provide good descriptions for average properties in the entrance channel before the system runs into instabilities, we thus believe our results of the dependence on the average properties, i.e., density, mass asymmetry and equation of state, which lead to the onset of multifragmentation, carry reliable information for such processes. Further efforts to include explicit correlations and fluctuations into BUU type models may provide more stringent test on the relative importance of thermal and dynamical instabilities.

The author would like to acknowledge C.A. Gagliardi, J.B. Natowitz, C.M. Ko, R. Schmitt, R.E. Tribble, and D.H. Youngblood, at Texas A&M University, and G.F. Bertsch, P. Danielewicz, C.K. Gelbke, and W.G. Lynch, at Michigan State University, for helpful discussions and advice. Critical reading and comments of the manuscript by J.B. Natowitz are greatly appreciated. This work was supported in part by the U.S. Department of Energy under Grant No. DE-FG05-86ER40256 and by the Robert A. Welch Foundation.

[1] D. Jacquet *et al.*, Phys. Rev. Lett. **53**, 2226 (1984).
[2] G. Auger *et al.*, Phys. Lett. **169B**, 161 (1986).
[3] J. Galin *et al.*, Phys. Rev. Lett. **48**, 1787 (1982).
[4] C.A. Ogilvie *et al.*, Phys. Rev. Lett. **67**, 1214 (1991).
[5] R.T. de Souza *et al.*, Phys. Lett. B **268**, 6 (1991).
[6] K. Hagel *et al.*, Phys. Rev. Lett. **68**, 2141 (1992).
[7] D.R. Bowman *et al.*, Phys. Rev. Lett. **67**, 1527 (1991).
[8] W.A. Friedman, Phys. Rev. Lett. **60**, 2125 (1988).
[9] R.J. Charity *et al.*, Nucl. Phys. **A483**, 371 (1987).
[10] J.P. Bondorf, R. Donangelo, I.N. Mishustin, C.J. Pethick, H. Schulz, and K. Sneppen, Nucl. Phys. **A443**, 321 (1985).
[11] D.H.E. Gross, Rep. Prog. Phys. **53**, 605 (1990); B.H. Sa, Y.M. Zheng, and X.Z. Zhang, Int. J. Mod. Phys. **A5**, 843 (1990).
[12] G. Bertsch and P.J. Siemens, Phys. Lett. **126B**, 9 (1983).
[13] D.H. Boal and A.L. Goodman, Phys. Rev. C **33**, 1690 (1986).
[14] J. Nemeth, M. Barranco, C. Ngô, and E. Tomasi, Z. Phys. A **320**, 691 (1985); J. Nemeth, M. Barranco, J. Desbois, and C. Ngô, *ibid.* **325**, 347(1986).
[15] D. Vautherin, J. Treiner, and M. Vénéroni, Phys. Lett. B **191**, 6 (1987).
[16] L. Vinet, F. Sébille, C. Grégoire, B. Remaud, and P. Schuck, Phys. Lett. B **172**, 17 (1986).
[17] B. Remaud, C. Grégoire, F. Sébille, and L. Vinet, Phys. Lett. B **180**, 198 (1986).
[18] B. Remaud, C. Grégoire, F. Sébille, and P. Schuck, Nucl. Phys. **A488**, 423c (1988).
[19] E. Suraud *et al.*, Phys. Lett. B **229**, 359 (1989).
[20] E. Suraud, C. Gregoire, and B. Tamain, Prog. Part. Nucl. Phys. **23**, 357 (1989).
[21] S.J. Lee, Phys. Lett. B **263**, 141 (1991); S.J. Lee, H.H. Gan, E.D. Cooper, and S. Das Gupta, Phys. Rev. C **41**, 706 (1990).
[22] L. De Paula, J. Nemeth, B.H. Sa, S. Leray, C. Ngô, H. Ngô, S.R. Souza, and Y.M. Zheng, Phys. Lett. B **258**, 251 (1991).
[23] M. Pi, E. Suraud, and P. Schuck, Nucl. Phys. **A524**, 537 (1991).

[24] F. Garcias, V. De La Mota, B. Remaud, G. Royer, and F. Sébille, Phys. Lett. B **255**, 311 (1991).

[25] L.G. Moretto, Kin Tso, N. Colonna, and G.J. Wozniak, Phys. Rev. Lett. **69**, 1884 (1992).

[26] H.M. Xu, W.G. Lynch, P. Danielewicz, and G.F. Bertsch, Phys. Rev. Lett. **65**, 843 (1990); Phys. Lett. B **261**, 240 (1991); H.M. Xu, P. Danielewicz, W.G. Lynch (unpublished).

[27] H.M. Xu, Phys. Rev. Lett. **67**, 2769 (1991); Phys. Rev. C **46**, R389 (1992).

[28] H.M. Xu *et al.*, (unpublished); H.M. Xu, Ph.D. dissertation, Michigan State University, 1991.

[29] G.F. Bertsch and S. Das Gupta, Phys. Rep. **160,** 189 (1988), and references therein.

[30] R.J. Lenk and V.R. Pandharipande, Phys. Rev. C **39**, 2242 (1989).

[31] Using the notations of Ref. [18], $E^*_{\rm exp}$ is defined as $E^*_{\rm exp} = \frac{2}{3}[E(T=0,\rho) - E(T=0,\rho=\rho_0)]$.

[32] The uncertainties due to the finite number of test particles were corrected for both the $E^*_{\rm coll}$ and $E^*_{\rm the}$, using a momentum analysis technique. For details see Ref. [28].

[33] We have investigated the numerical accuracy of using the decomposition technique of Ref. [18]. By preparing ground state nuclei with masses $A = 40$–124 and turning off the collision term to prevent heat production, we have determined the various components to be accurate to within 0.4 MeV per nucleon over a period of 240 fm/c. In addition, statistical uncertainties estimated are less than 0.3 MeV per nucleon and are, for clarity, not shown in Fig. 4.

[34] The minimum perturbations and fluctuations are mainly provided by the random cascades of two-body collisions.